



# CRAB Pulse Optimization for Transmon CNOT Gate with Leakage and Decoherence

Ridhwan Dery Iradat<sup>1\*</sup>, Juri Pebrianto<sup>1</sup>

<sup>1</sup> Physics Study Program, Syarif Hidayatullah State Islamic University Jakarta, South Tangerang 15412, Indonesia.

<sup>1</sup> Information Technology Study Program, Syarif Hidayatullah State Islamic University Jakarta, South Tangerang 15412, Indonesia.

DOI: <https://doi.org/10.29303/goescienceed.v7i3.2433>

## Article Info:

Received : May, 20 2026

Revised : June, 15 2026

Accepted : June, 26 2026

Published : July, 03 2026

## Correspondence:

Ridhwan Dery Iradat

Phone: +6281261372729

**Abstract:** High-fidelity two-qubit gates are essential for scalable quantum computation in superconducting transmon circuits. However, weak anharmonicity can induce leakage outside the computational subspace, while relaxation and dephasing reduce gate fidelity. This study presents a numerical simulation of a CNOT gate in a coupled two-transmon system. Each transmon is modeled as a three-level system, where  $|0\rangle$  and  $|1\rangle$  form the computational subspace, while  $|2\rangle$  is included to evaluate leakage. The control pulses are optimized using a two-channel chopped random basis (CRAB) method. The pulse  $u_1(t)$  is applied to the control transmon as the main drive, while  $u_2(t)$  is applied to the target transmon as a correction drive. The system is simulated under closed- and open-system conditions. In the open system, energy relaxation and pure dephasing are included through the Lindblad master equation. CRAB optimization improves the CNOT basis fidelity from 0.65 to 0.96 in the closed system and from 0.65 to 0.95 in the open system. The final leakage remains small, around  $10^{-3}$ . These results indicate that the correction drive can improve CNOT gate performance while keeping leakage low.

**Keywords:** CNOT; Transmon; CRAB; Optimization; Lindblad; Leakage.

**Citation:** Iradat, R. D., & Pebrianto, J. (2026). CRAB Pulse Optimization for Transmon CNOT Gate with Leakage and Decoherence . *Jurnal Pendidikan, Sains, Geologi, Dan Geofisika (GeoScienceEd Journal)*, 7(3), 3094–3102. <https://doi.org/10.29303/goescienceed.v7i3.2433>

## Introduction

Quantum Quantum gates are basic operations in quantum information processing because they control the amplitude, coherence, and relative phase of quantum states. In quantum circuits, single-qubit gates and two-qubit gates are required to construct more complex quantum operations. Among the two-qubit gates, the controlled-NOT (CNOT) gate is particularly important because, together with single-qubit gates, it forms a universal gate set for quantum computation and is widely used for circuit synthesis, entanglement generation, and quantum error correction (Krantz et al., 2019; Ma et al., 2018; Maslov & Zindorf, 2022). Since a CNOT gate directly creates conditional two-qubit dynamics, small control errors, leakage to noncomputational states, and decoherence can strongly reduce the reliability of the resulting quantum circuit. Therefore, improving the fidelity of the CNOT gate is

essential for building more accurate and scalable quantum processors.

Although several methods have been proposed to realize high-fidelity two-qubit gates in superconducting circuits, maintaining high fidelity in weakly anharmonic transmon systems remains challenging (Krantz et al., 2019; Kirchhoff et al., 2018; Patterson et al., 2019). The weak anharmonicity of transmons makes the system susceptible to leakage from the computational subspace, especially when strong or fast control pulses are applied. In addition, many pulse-design studies focus mainly on closed-system dynamics, while realistic gate performance must also be evaluated under open-system effects such as energy relaxation and pure dephasing (Manzano, 2020; Chen et al., 2025). Based on this gap, this study investigates a two-channel CRAB optimization scheme for a CNOT gate in a coupled two-transmon system modeled beyond the ideal two-level

Email: [ridhwandery.official@gmail.com](mailto:ridhwandery.official@gmail.com)

approximation. The novelty of this work lies in combining a three-level transmon model, two-channel CRAB pulse correction, and closed and open system evaluation to analyze fidelity improvement and leakage suppression simultaneously.

Superconducting circuits are one of the main platforms used to realize quantum gates. In this platform, quantum states are formed from circuit variables, such as superconducting phase and Cooper pair number, so the qubit properties can be engineered through circuit design (Krantz et al., 2019; Leonard et al., 2019). The transmon qubit is commonly used because it has lower sensitivity to charge noise compared with the charge qubit. The basic Hamiltonian of a transmon can be expressed as follows

$$H = 4E_C(\hat{n} - n_g)^2 - E_J \cos \hat{\phi},$$

where  $E_C$  represents the charging energy,  $E_J$  represents the Josephson energy,  $\hat{n}$  is the Cooper-pair number operator,  $n_g$  is the offset charge, and  $\hat{\phi}$  is the superconducting phase operator. In the regime  $E_J \gg E_C$ , the transmon can be approximated as a weakly anharmonic oscillator. Therefore, the two lowest energy levels,  $|0\rangle$  and  $|1\rangle$ , are used as the computational subspace of the qubit. (Krantz et al., 2019).

Although the transmon is commonly treated as a qubit, physically it is a multilevel system. This means that higher excited states, especially  $|2\rangle$ , may still influence the gate dynamics when the control pulse is not designed carefully. Population transfer from the computational subspace to higher states is known as leakage, and it can reduce gate fidelity (Goss et al., 2022; Kandala et al., 2021). **Figure 1** illustrates the transmon energy ladder, where the level spacing is not uniform because of the weak anharmonicity. In this work, the levels  $|0\rangle$  and  $|1\rangle$  are used as the computational basis, while  $|2\rangle$  is included in the model to capture the possibility of leakage. Thus, the system is not treated as an ideal two levels of qubit, but as a more realistic three levels of transmon model.

To construct a CNOT gate, two transmons must interact through an effective coupling. In fixed frequency transmon architectures, two qubit gates are commonly realized using microwave driven interactions, such as the cross-resonance mechanism, in which one transmon is driven near the transition frequency of the other to produce an effective two qubit coupling (Kirchhoff et al., 2018; Patterson et al., 2019). In this system, one transmon can be used as the control qubit, while the other transmon acts as the target qubit. The resulting gate performance depends not only on the desired interaction itself, but also on the detailed pulse shape and on non ideal effects such as unwanted

couplings, static ZZ interaction, crosstalk, frequency crowding, and leakage to non computational levels (Kandala et al., 2021; Klimov et al., 2024; Stehlik et al., 2021).

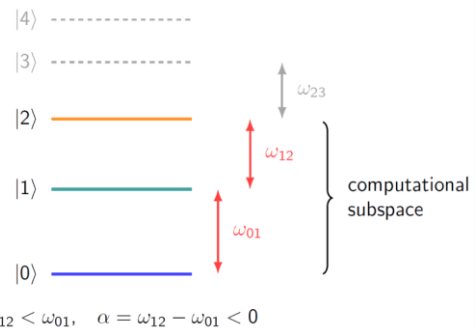


**Figure 1.** Transmon energy ladder as a weakly anharmonic oscillator.

For this reason, quantum optimal control becomes important in designing control pulses that can drive the system close to the desired target operation. In quantum optimal control, the pulse parameters are adjusted to maximize gate fidelity or minimize an error functional (Huang & Goan, 2014; Abdelhafez et al., 2020). One practical method is the chopped random basis (CRAB) method, in which the control pulse is expanded in a limited number of basis functions, so the optimization can be performed using a relatively small set of parameters (Caneva et al., 2011). This method is suitable for simple numerical studies and is also relevant for physical implementations because realistic microwave pulses are constrained by finite amplitude, bandwidth, and time resolution (Rach et al., 2015; Chen et al., 2025). In addition, in transmon systems the pulse must not be excessively strong or too rapid, since that can enhance leakage and other coherent errors (Goss et al., 2022; Kirchhoff et al., 2018).

Based on this background, this study performs a numerical investigation of a CNOT gate in a system of two coupled three-level transmons. The first transmon is treated as the control qubit, while the second transmon is treated as the target qubit. Each transmon is modeled using the three lowest energy levels, where  $|0\rangle$  and  $|1\rangle$  form the computational subspace, while  $|2\rangle$  is included to observe leakage.

Two control pulses are used in this study. The pulse  $u_1(t)$  is applied to the control transmon as the main drive, while  $u_2(t)$  is applied to the target transmon as a correction drive inspired by the cancellation-tone concept in cross-resonance gates (Alexander et al., 2020; Patterson et al., 2019). The pulse shapes are optimized using the CRAB method. The performance of the gate is evaluated from the CNOT basis fidelity, which describes how close the final state transformation is to the ideal CNOT operation, and from the leakage outside the

computational subspace. This study considers both closed and open system dynamics, where the open system model includes energy relaxation and pure dephasing through the Lindblad master equation (Manzano, 2020; Chen et al., 2025). Therefore, the main objective of this work is to analyze how dual-control CRAB pulses affect population dynamics, leakage, and CNOT gate fidelity in a coupled two-transmon system.

### Method

The numerical simulation is performed for a CNOT gate in a system of two coupled transmons. Each transmon is modeled as a three-level system consisting of  $|0\rangle$ ,  $|1\rangle$ , and  $|2\rangle$ . The levels  $|0\rangle$  and  $|1\rangle$  are used as the computational subspace, while the level  $|2\rangle$  is included to observe possible population leakage. This three-level model is used because a transmon is not an ideal two-level qubit. Due to its finite anharmonicity, population may be transferred to a non-computational level during the pulse-driven gate operation (Krantz et al., 2019; Goss et al., 2022). The Hilbert space of the system is written as

$$\mathcal{H} = \mathbb{C}^3 \otimes \mathbb{C}^3,$$

so the total dimension of the system is 9.

In this simulation, the first transmon is assigned as the control qubit, while the second transmon is assigned as the target qubit. The four computational basis states, namely  $|00\rangle$ ,  $|01\rangle$ ,  $|10\rangle$ , and  $|11\rangle$ , are used as the input states. The target operation follows the ideal CNOT mapping,

$$\begin{aligned} |00\rangle &\rightarrow |00\rangle, & |01\rangle &\rightarrow |01\rangle, \\ |10\rangle &\rightarrow |11\rangle, & |11\rangle &\rightarrow |10\rangle. \end{aligned}$$

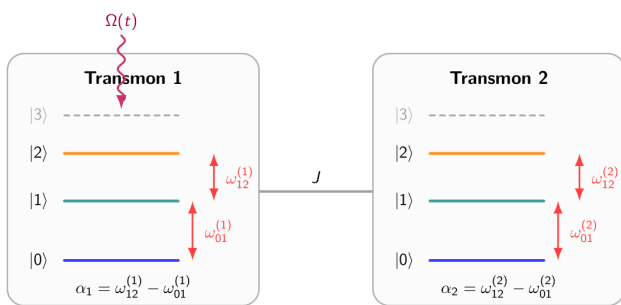


**Figure 2.** Conceptual scheme of two coupled three-level transmons. Transmon 1 acts as the control qubit, while Transmon 2 acts as the target qubit.

Based on this operation, the target qubit changes its state only when the control qubit is in the state  $|1\rangle$ . If the control qubit is in the state  $|0\rangle$ , the state of the target qubit remains the same.

The system Hamiltonian is written in a rotating frame. This frame removes the fast microwave carrier

oscillation at the GHz scale, so the simulation only needs to calculate the slower dynamics of the pulse envelope. The total Hamiltonian used in this study is

$$H(t) = H_0 + u_1(t)H_{c,1} + u_2(t)H_{c,2},$$

where the drift Hamiltonian is given by

$$H_0 = \sum_{j=1}^2 \left[ \delta_j \hat{n}_j + \frac{\alpha_j}{2} \hat{n}_j (\hat{n}_j - \hat{I}) \right] + J(\hat{b}_1^\dagger \hat{b}_2 + \hat{b}_1 \hat{b}_2^\dagger).$$

Here,  $\hat{b}_j$  is the annihilation operator of the  $j$ -th transmon,  $\hat{n}_j = \hat{b}_j^\dagger \hat{b}_j$  is the excitation number operator,  $\alpha_j$  is the anharmonicity, and  $J$  is the coupling strength between the two transmons. The detuning is defined as  $\delta_j = \omega_j - \omega_d$ , where  $\omega_d$  is the drive frequency. In this study, the drive frequency is chosen to be close to the target-transmon frequency. In the numerical implementation,  $\omega_d = \omega_2$  is used, so that  $\delta_2 = 0$ .

Two control pulses are applied to the system through the control operators

$$H_{c,j} = \frac{1}{2}(\hat{b}_j + \hat{b}_j^\dagger), \quad j = 1,2.$$

The first control channel,  $u_1(t)$ , is applied to the first transmon as the main drive. The second control channel,  $u_2(t)$ , is applied to the second transmon as a correction drive. The use of these two channels is inspired by the cross-resonance gate. In this mechanism, a microwave drive applied to the control qubit can generate an effective two-qubit interaction, but it may also produce unwanted rotations on the target qubit. To reduce this unwanted effect, cross-resonance implementations can use a cancellation tone on the target qubit (Patterson et al., 2019; Alexander et al., 2020). Therefore, in this study,  $u_2(t)$  is treated as a correction channel and optimized together with  $u_1(t)$ .

The system dynamics are calculated under two conditions. The first condition is the closed system case, where the evolution is determined only by the Hamiltonian  $H(t)$ . The second condition is the open system case, where the evolution is affected by energy relaxation and pure dephasing. For the open system, the density matrix  $\rho$  is evolved using the Lindblad master equation

In these equations,  $T_1$  represents the energy relaxation time, while  $T_\phi$  represents the pure dephasing time. Energy relaxation describes the loss of excitation from the qubit to the environment, whereas pure dephasing describes the loss of phase coherence without directly changing the population. The Lindblad

equation is used because it is a standard approach for modeling Markovian open quantum systems interacting with an environment (Manzano, 2020; Chen et al., 2025).

$$\dot{\rho} = -i[H(t), \rho] + \sum_{j=1}^2 \mathcal{D} \left[ \sqrt{\frac{1}{T_{1,j}}} \hat{b}_j \right] \rho + \sum_{j=1}^2 \mathcal{D} \left[ \sqrt{\frac{2}{T_{\phi,j}}} \hat{n}_j \right] \rho$$

The dissipation superoperator is defined as

$$\mathcal{D}[L]\rho = L\rho L^\dagger - \frac{1}{2}(L^\dagger L\rho + \rho L^\dagger L)$$

The control pulses  $u_1(t)$  and  $u_2(t)$  are optimized using the chopped random basis, or CRAB, method. In this method, the pulse is not treated as a fully free function. Instead, it is expanded using a finite number of sine and cosine functions. This makes the optimization simpler because only a limited number of coefficients need to be optimized. For the  $j$ -th control channel, the pulse is written as

$$u_j(t) = u_{\max,j} S(t) [c_{j,0} + \sum_{k=1}^{N_c} (A_{j,k} \sin(v_{j,k}t) + B_{j,k} \cos(v_{j,k}t))]'$$

with the envelope function

$$S(t) = \sin^2\left(\frac{\pi t}{T_g}\right).$$

This envelope forces the pulse to be zero at the beginning and at the end of the gate, so the pulse turns on and off smoothly. In Equation (9),  $c_{j,0}$ ,  $A_{j,k}$ , and  $B_{j,k}$  are the optimized coefficients. The basis frequencies  $v_{j,k}$  are slightly randomized from the main Fourier modes to provide more flexibility in the pulse shape. The CRAB method is chosen because it transforms a time dependent pulse optimization problem into an optimization problem with a finite number of parameters (Caneva et al., 2011; Rach et al., 2015).

The CNOT performance is evaluated using the average basis-state fidelity over the four computational input states. If  $\rho_m(T_g)$  is the final state for the  $m$ -th input and  $|\psi_m^{\text{tar}}\rangle$  is the corresponding target state from the ideal CNOT mapping, then the basis-state fidelity is written as

$$F_{\text{basis}} = \frac{1}{4} \sum_m \langle \psi_m^{\text{tar}} | \rho_m(T_g) | \psi_m^{\text{tar}} \rangle,$$

where  $m \in \{00,01,10,11\}$ . A fidelity value close to one indicates that the final states are close to the ideal CNOT output states.

In addition to fidelity, this study also calculates leakage. Leakage represents the population that leaves the computational subspace. The computational subspace consists only of the states  $|00\rangle$ ,  $|01\rangle$ ,  $|10\rangle$ , and  $|11\rangle$ . For each input state, leakage is calculated as

$$P_{\text{leak}}^{(m)}(t) = 1 - \text{Tr}[P_c \rho_m(t)],$$

With

$$P_c = \sum_m |m\rangle \langle m|, \quad m \in \{00,01,10,11\}.$$

The average leakage over the four computational inputs is then written as

$$\bar{P}_{\text{leak}}(t) = \frac{1}{4} \sum_m P_{\text{leak}}^{(m)}(t).$$

Based on this definition, any population in states involving the level  $|2\rangle$  is counted as leakage. A smaller leakage value means that the control pulse is better at keeping the population inside the computational subspace.

The CRAB coefficients are obtained by minimizing the objective function

$$J = 1 - F_{\text{basis}} + \lambda_L \bar{P}_{\text{leak}}(T_g) + \lambda_E \frac{1}{2T_g} \sum_{j=1}^2 \int_0^{T_g} |u_{\max,j}(t)|^2 dt.$$

The first term guides the system toward the target CNOT operation, the second term penalizes leakage, and the third term limits the pulse energy. The optimization is first performed in the closed-system case to obtain the CRAB pulse. After that, the optimized pulse is tested again in the open system case by including relaxation and dephasing. With this procedure, the ideal performance and the performance under decoherence can be compared.

The numerical parameters used in this study are shown in **Table 1**. The transmon frequencies, anharmonicities, coupling strength,  $T_1$ , and  $T_\phi$  are based on the two-transmon cross-resonance device studied by Patterson et al. (2019). The gate time is chosen as  $T_g = 180$  ns because it is on the same order as CNOT implementations in fixed-frequency transmons (Kandala et al., 2021). The number of CRAB modes is chosen as  $N_c = 6$  to give enough pulse flexibility while keeping the number of optimization parameters limited.

The amplitude limits,  $u_{\max,1}/2\pi = 100$  MHz and  $u_{\max,2}/2\pi = 80$  MHz, are chosen in the range of tens to hundreds of MHz, which is consistent with the microwave-control scale used in superconducting-circuit pulse optimization (Kirchhoff et al., 2018; Chen et al., 2025). In the numerical implementation, all frequencies are converted into angular frequencies using  $\omega = 2\pi f$ .

**Table 1.** Numerical parameters used in the dual control simulation.

Parameters	Symbols	Values
Levels per transmon	$N$	3
Transmon 1 frequency	$\omega_1/2\pi$	6.509 GHz
Transmon 2 frequency	$\omega_2/2\pi$	5.963 GHz
Drive frequency	$\omega_d/2\pi$	5.963 GHz
Transmon 1 anharmonicity	$\alpha_1/2\pi$	-300 MHz
Transmon 2 anharmonicity	$\alpha_2/2\pi$	-314 MHz
Interqubit coupling	$J/2\pi$	10.7 MHz
Relaxation time 1	$T_{1,1}$	16.2 $\mu$ s
Relaxation time 2	$T_{1,2}$	23.9 $\mu$ s
Pure dephasing time 1	$T_{\phi,1}$	111 $\mu$ s
Pure dephasing time 2	$T_{\phi,2}$	134 $\mu$ s
Gate time	$T_g$	180 ns
Time step	$\Delta t$	0.5 ns
CRAB modes per channel	$N_c$	6
Main drive amplitude limit	$u_{\max,1}/2\pi$	100 MHz
Correction drive amplitude limit	$u_{\max,2}/2\pi$	80 MHz
Leakage penalty	$\lambda_L$	$5 \times 10^{-2}$
Energy penalty	$\lambda_E$	$10^{-5}$
Optimization restarts	-	4
Iterations per restart	-	800

The parameters are adapted from superconducting-transmon, cross resonance, and quantum control studies (Krantz et al., 2019; Goss et al., 2022; Patterson et al., 2019; Kandala et al., 2021; Caneva et al., 2011; Rach et al., 2015; Kirchhoff et al., 2018; Chen et al., 2025).

## Result and Discussion

The simulation was performed to evaluate the performance of a CNOT gate in a system of two three-level transmons using two channel CRAB pulse optimization. The channel  $u_1(t)$  is applied to the control transmon as the main drive, while the channel  $u_2(t)$  is applied to the target transmon as a correction drive. The use of these two channels is inspired by the cross-resonance gate. In this gate, a drive on the control qubit can generate a two qubit interaction, but it can also produce unwanted local rotations on the target qubit (Patterson et al., 2019; Alexander et al., 2020). Therefore,

the second channel is used to help correct the target dynamics so that the final result becomes closer to the ideal CNOT transformation.

The main simulation results are shown in **Table 2**. In the closed system, the initial pulse gives a CNOT basis fidelity of 0.65 with an average final leakage of  $1.51 \times 10^{-3}$ . After two-channel CRAB optimization, the fidelity increases to 0.96, while the average final leakage becomes  $2.27 \times 10^{-3}$ . These results show that the CRAB pulse can produce a much better gate dynamics than the initial pulse. In terms of infidelity,  $1 - F_{\text{basis}}$ , the error decreases from 0.35 to 0.04. Thus, the two-channel CRAB optimization successfully reduces the basis-state error. This result is consistent with the purpose of the CRAB method, which is to find an optimal pulse shape using a small number of parameters in sine and cosine bases (Caneva et al., 2011; Rach et al., 2015).

**Table 2:** Comparison of CNOT basis fidelity and average final leakage for the initial pulse and the two channel CRAB pulse.

Case	$F_{\text{basis}}$	$P_{\text{leak}}(T_g)$
Initial closed system	0.65	$1.51 \times 10^{-3}$
CRAB closed system	0.96	$2.27 \times 10^{-3}$
Initial open system	0.65	$1.50 \times 10^{-3}$
CRAB open system	0.95	$2.30 \times 10^{-3}$

The initial pulse and the optimized pulse are shown in **Figure 3**. In the initial pulse, the main channel  $u_1(t)$  is applied to the control transmon, while the correction channel  $u_2(t)$  on the target transmon is still zero. After optimization,  $u_1(t)$  becomes the dominant main pulse. At the same time,  $u_2(t)$  becomes active and forms a correction pulse. This shows that CRAB uses the additional channel on the target transmon to improve the gate dynamics. Physically, this result is consistent with the concept of a cancellation tone in the cross-resonance gate, where an additional correction is applied to the target qubit to suppress unwanted local rotations (Patterson et al., 2019; Alexander et al., 2020).

The optimization process is shown by the fidelity curve in **Figure 4**. The curve shows that the best fidelity increases gradually during the CRAB parameter search. Some local decreases in fidelity appear at certain iterations because the optimization uses several restarts from different initial parameters. Therefore, these local decreases do not mean that the optimization fails, but are part of the search strategy to obtain a better solution. The best-fidelity curve shows that the optimization finds a pulse with a maximum basis fidelity of 0.96 in the closed system.

In the open system, the fidelity of the initial pulse is 0.65, while the fidelity of the CRAB pulse is 0.95. This value is slightly lower than the result in the closed

system. For the optimized pulse, the fidelity decrease from the closed system to the open system is 0.01. This decrease is relatively small. It means that energy relaxation and pure dephasing are not the main limiting factors for the gate time  $T_g = 180$  ns and the coherence parameters used in this study. In other words, the CRAB pulse obtained from closed system optimization still performs well when tested in the open system using the Lindblad master equation (Manzano, 2020; Chen et al., 2025).

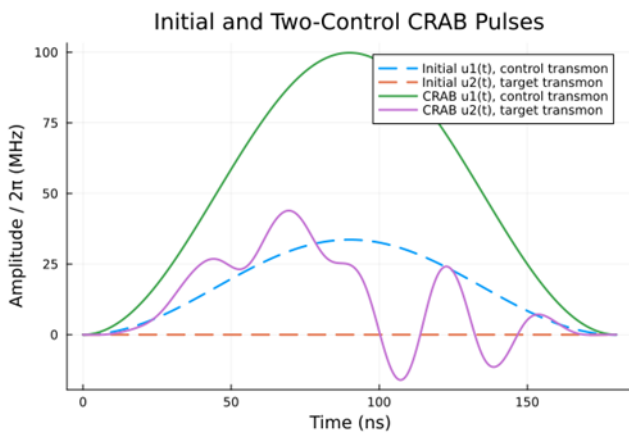


**Figure 3.** Initial pulse and optimized two channel CRAB pulse.

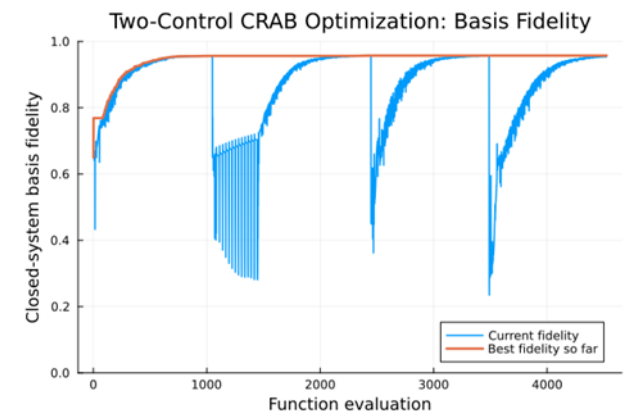
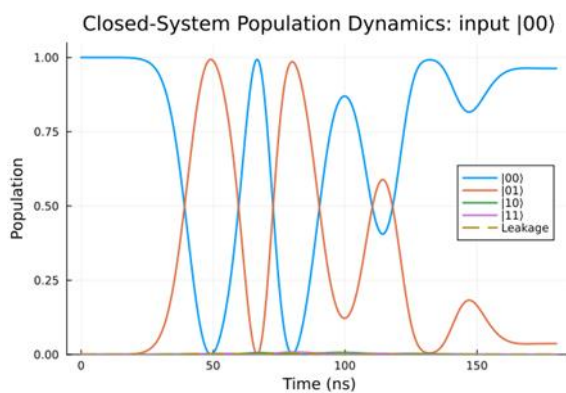


**Figure 4.** CNOT basis fidelity curve during the two-channel CRAB optimization process.

The leakage after optimization is slightly larger than that of the initial pulse, but it remains on the order of  $10^{-3}$ . In the closed system, the average final leakage changes from  $1.51 \times 10^{-3}$  to  $2.27 \times 10^{-3}$ . In the open system, the average final leakage after optimization is  $2.30 \times 10^{-3}$ . This value is still small, so the increase in fidelity is not accompanied by a large population leakage to non-computational levels. This is important because a transmon has limited anharmonicity. Therefore, the level  $|2\rangle$  must still be included in the model to evaluate leakage during the gate process (Krantz et al., 2019; Goss et al., 2022).

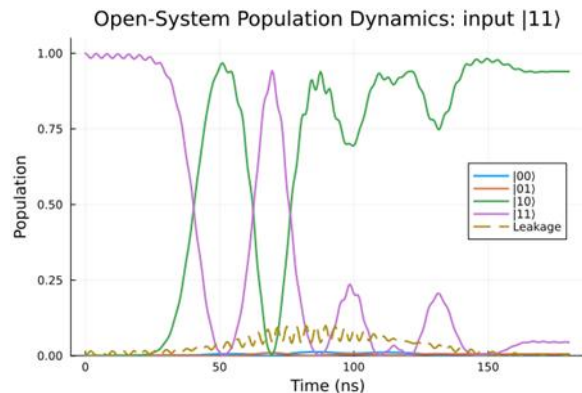


**Figure 5.** Representative population dynamics in the closed system after two-channel CRAB optimization. The left panel shows the input  $|00\rangle$ , where the target state does not change. The right panel shows the input  $|11\rangle$ , which represents the conditional flip case toward  $|10\rangle$ . The leakage curve shows the population that leaves the computational subspace.

The analysis for each CNOT input is shown in **Table 3**. For the inputs  $|00\rangle$  and  $|01\rangle$ , the final fidelities are 0.96 and 0.96, respectively. These two inputs represent the condition where the control qubit is in the state  $|0\rangle$ , so the target qubit does not need to flip. For the inputs  $|10\rangle$  and  $|11\rangle$ , the final fidelities are 0.95 and 0.95, respectively. These two inputs are more difficult because the target qubit must flip when the control qubit is in the state  $|1\rangle$ . The largest leakage appears for the input  $|11\rangle$ , with a value of  $5.12 \times 10^{-3}$ . Thus, the

transition  $|11\rangle \rightarrow |10\rangle$  becomes the most challenging part in the CNOT gate formation in this simulation.

The representative population dynamics are shown in **Figure 5**. The input  $|00\rangle$  is chosen to represent the case where the control qubit is in the state  $|0\rangle$ , so the target qubit does not change. In this case, the final population remains dominant in the state  $|00\rangle$ , which agrees with the CNOT rule. In contrast, the input  $|11\rangle$  is chosen to represent the more difficult conditional flip case. In this case, the population mainly moves to the

state  $|10\rangle$ , which is the CNOT target state. The leakage curve for the input  $|11\rangle$  is larger than that for the input  $|00\rangle$ , consistent with the results in **Table 3**. Therefore, the population dynamics support the result that the two-channel CRAB pulse can produce the CNOT mapping in the computational basis.

**Table 3.** Final fidelity and leakage for each CNOT input in the closed system after two channel CRAB optimization.

Input	Fidelity	Leakage
$ 00\rangle$	0.96	$1.35 \times 10^{-13}$
$ 01\rangle$	0.96	$1.52 \times 10^{-6}$
$ 10\rangle$	0.95	$3.98 \times 10^{-3}$
$ 11\rangle$	0.95	$5.12 \times 10^{-3}$

The summary of fidelity and leakage is shown in **Figure 6**. The fidelity panel shows that CRAB optimization improves the gate performance in both the closed and open systems. The leakage panel shows that the final leakage after optimization slightly increases,

but it remains on the order of  $10^{-3}$ . Therefore, the fidelity improvement is not obtained at the cost of large leakage. This figure supports the results in **Table 3**, showing that the two channel CRAB pulse gives a clear performance improvement while keeping the non computational population small.

In summary, the simulation results show that two-channel CRAB optimization can improve the performance of the CNOT gate in two coupled transmons. The basis fidelity increases from about 0.65 to about 0.96 in the closed system, and remains around 0.95 in the open system. The final leakage remains small, on the order of  $10^{-3}$ . These results show that the combination of the main drive on the control transmon and the correction drive on the target transmon can be a relevant strategy to improve the quality of a transmon based CNOT gate. However, it should be noted that the fidelity used in this study is the CNOT basis fidelity, not the full process fidelity. Therefore, these results should be understood as an initial evaluation of the success of the four computational-basis transformations.

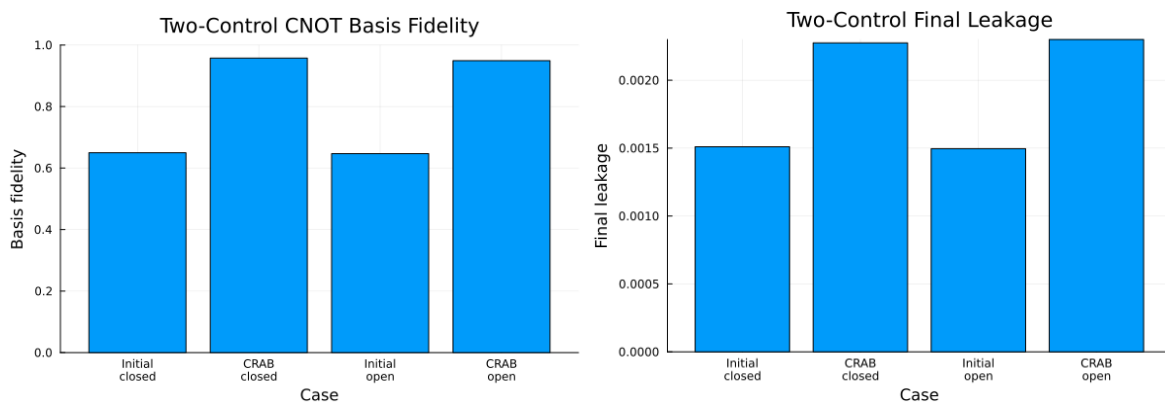


**Figure 6.** Summary of CNOT gate performance for the initial pulse and the two channel CRAB pulse. The left panel shows the basis fidelity in the closed and open systems. The right panel shows the final leakage. CRAB optimization significantly improves the fidelity, while the leakage remains on the order of  $10^{-3}$ .

### Conclusion

This study has performed a numerical simulation of a CNOT gate in a system of two three-level transmons using two channel CRAB pulse optimization. The first transmon is used as the control qubit, while the second transmon is used as the target qubit. The channel  $u_1(t)$  acts as the main drive on the control transmon, while the channel  $u_2(t)$  acts as a correction drive on the target transmon. The three-level model is used so that leakage to the non computational level  $|2\rangle$  can be observed. The effects of energy relaxation and pure dephasing are also included through the Lindblad master equation.

The simulation results show that two channel CRAB optimization can clearly improve the CNOT basis fidelity. In the closed system, the fidelity increases from 0.65 to 0.96. In the open system, the fidelity increases from 0.65 to 0.95. The fidelity decrease from the closed

system to the open system is only about 0.01, indicating that decoherence is not yet the main limiting factor for the parameters used in this study. The final leakage after optimization also remains small, on the order of  $10^{-3}$ . Therefore, the fidelity improvement is not accompanied by a large population leakage. For future development, the gate evaluation can be extended by using process fidelity or average gate fidelity, instead of only the CNOT basis fidelity (Alexander et al., 2020; Kandala et al., 2021). The optimization can also be performed directly in the open-system model, so that relaxation and dephasing effects are included during the pulse-search process (Manzano, 2020; Chen et al., 2025). In addition, the CRAB method can be compared with other methods such as dCRAB, GRAPE, or Krotov, and the optimized gate can be tested under variations of gate time, pulse amplitude, detuning, interqubit coupling, and

decoherence parameters (Caneva et al., 2011; Rach et al., 2015; Kirchhoff et al., 2018; Patterson et al., 2019; Wittler et al., 2021).

## Acknowledgements

The authors gratefully acknowledge the Faculty of Science and Technology, UIN Syarif Hidayatullah Jakarta, for providing support, facilities, and academic encouragement during the completion of this research.

## References

- Abdelhafez, M., Baker, B., Gyenis, A., Mundada, P., Houck, A. A., Schuster, D., & Koch, J. (2020). Universal gates for protected superconducting qubits using optimal control. *Physical Review A*, 101, 022321. <https://doi.org/10.1103/PhysRevA.101.022321>
- Alexander, T., Kanazawa, N., Egger, D. J., Capelluto, L., Wood, C. J., Javadi-Abhari, A., & McKay, D. C. (2020). Qiskit pulse: Programming quantum computers through the cloud with pulses. *Quantum Science and Technology*, 5, 044006. <https://doi.org/10.1088/2058-9565/aba404>
- Ann, B.-M., & Steele, G. A. (2024). All-microwave Lamb shift engineering for a fixed frequency multi-level superconducting qubit. *Communications Physics*, 7, 347. <https://doi.org/10.1038/s42005-024-01841-0>
- Caneva, T., Calarco, T., & Montangero, S. (2011). Chopped random-basis quantum optimization. *Physical Review A*, 84, 022326. <https://doi.org/10.1103/PhysRevA.84.022326>
- Chen, Z.-J., Huang, H., Sun, L., Jie, Q.-X., Zhou, J., Hua, Z., Xu, Y., Wang, W., Guo, G.-C., Zou, C.-L., Sun, L., & Zou, X.-B. (2025). Robust and optimal control of open quantum systems. *Science Advances*, 11, eadr0875. <https://doi.org/10.1126/sciadv.adr0875>
- Goss, N., Morvan, A., Marinelli, B., Mitchell, B. K., Nguyen, L. B., Naik, R. K., Chen, L., Jünger, C., Kreikebaum, J. M., Santiago, D. I., Wallman, J., & Siddiqi, I. (2022). High-fidelity qutrit entangling gates for superconducting circuits. *Nature Communications*, 13, 7481. <https://doi.org/10.1038/s41467-022-34851-z>
- Huang, S.-Y., & Goan, H.-S. (2014). Optimal control for fast and high-fidelity quantum gates in coupled superconducting flux qubits. *Physical Review A*, 90, 012318. <https://doi.org/10.1103/PhysRevA.90.012318>
- Kandala, A., Wei, K. X., Srinivasan, S., Magesan, E., Carnevale, S., Keefe, G. A., Klaus, D., Dial, O., & McKay, D. C. (2021). Demonstration of a high-fidelity CNOT gate for fixed-frequency transmons with engineered ZZ suppression. *Physical Review Letters*, 127, 130501. <https://doi.org/10.1103/PhysRevLett.127.130501>
- Kirchhoff, S., Keßler, T., Liebermann, P. J., Assémat, E., Machnes, S., Motzoi, F., & Wilhelm, F. K. (2018). Optimized cross-resonance gate for coupled transmon systems. *Physical Review A*, 97, 042348. <https://doi.org/10.1103/PhysRevA.97.042348>
- Klimov, P. V., Bengtsson, A., Quintana, C., Bourassa, A., Hong, S., Dunsworth, A., Satzinger, K. J., Livingston, W. P., Sivak, V., Niu, M. Y., Andersen, T. I., Zhang, Y., Chik, D., Chen, Z., Neill, C., Erickson, C., Grajales Dau, A., Megrant, A., ... Neven, H. (2024). Optimizing quantum gates towards the scale of logical qubits. *Nature Communications*, 15, 2442. <https://doi.org/10.1038/s41467-024-46623-y>
- Krantz, P., Kjaergaard, M., Yan, F., Orlando, T. P., Gustavsson, S., & Oliver, W. D. (2019). A quantum engineer's guide to superconducting qubits. *Applied Physics Reviews*, 6, 021318. <https://doi.org/10.1063/1.5089550>
- Lane, J. R., Tan, D., Beysengulov, N. R., Nasyedkin, K., Brook, E., Zhang, L., Stefanski, T., Byeon, H., Murch, K. W., & Pollanen, J. (2020). Integrating superfluids with superconducting qubit systems. *Physical Review A*, 101, 012336. <https://doi.org/10.1103/PhysRevA.101.012336>
- Leonard, E., Jr., Beck, M. A., Nelson, J., Christensen, B. G., Thorbeck, T., Howington, C., Opremcak, A., Pechenezhskiy, I. V., Dodge, K., Dupuis, N. P., Hutchings, M. D., Ku, J., Schlenker, F., Suttle, J., Wilen, C., Zhu, S., Vavilov, M. G., Plourde, B. L. T., & McDermott, R. (2019). Digital coherent control of a superconducting qubit. *Physical Review Applied*, 11, 014009. <https://doi.org/10.1103/PhysRevApplied.11.014009>
- Ma, L.-H., Kang, Y.-H., Shi, Z.-C., Song, J., & Xia, Y. (2018). Shortcuts to adiabatic for implementing controlled-not gate with superconducting quantum interference device qubits. *Quantum Information Processing*, 17, 292. <https://doi.org/10.1007/s11128-018-2056-x>
- Manzano, D. (2020). A short introduction to the Lindblad master equation. *AIP Advances*, 10, 025106. <https://doi.org/10.1063/1.5115323>
- Maslov, D., & Zindorf, B. (2022). Depth optimization of CZ, CNOT, and Clifford circuits. *IEEE Transactions on Quantum Engineering*, 3, 3101

2500408.

<https://doi.org/10.1109/TQE.2022.3180900>

Patterson, A. D., Rahamim, J., Tsunoda, T., Spring, P. A., Jebari, S., Ratter, K., Mergenthaler, M., Tancredi, G., Vlastakis, B., Esposito, M., & Leek, P. J. (2019). Calibration of a cross-resonance two-qubit gate between directly coupled transmons. *Physical Review Applied*, 12, 064013. <https://doi.org/10.1103/PhysRevApplied.12.064013>

Rach, N., Müller, M. M., Calarco, T., & Montangero, S. (2015). Dressing the chopped-random-basis optimization: A bandwidth-limited access to the trap-free landscape. *Physical Review A*, 92, 062343. <https://doi.org/10.1103/PhysRevA.92.062343>

Sirois, A. J., Castellanos-Beltran, M., Fox, A. E., Benz, S. P., & Hopkins, P. F. (2020). Josephson microwave sources applied to quantum information systems. *IEEE Transactions on Quantum Engineering*, 1, 6002807. <https://doi.org/10.1109/TQE.2020.3045682>

Stehlik, J., Zajac, D. M., Underwood, D. L., Phung, T., Blair, J., Carnevale, S., Klaus, D., Keefe, G. A., Carniol, A., Kumph, M., Steffen, M., & Dial, O. E. (2021). Tunable coupling architecture for fixed-frequency transmon superconducting qubits. *Physical Review Letters*, 127, 080505. <https://doi.org/10.1103/PhysRevLett.127.080505>

Wittler, N., Roy, F., Pack, K., Werninghaus, M., Saha Roy, A., Egger, D. J., Filipp, S., Wilhelm, F. K., & Machnes, S. (2021). Integrated tool set for control, calibration, and characterization of quantum devices applied to superconducting qubits. *Physical Review Applied*, 15, 034080. <https://doi.org/10.1103/PhysRevApplied.15.034080>